Highlights

Model Predictive Approaches for Cost-Efficient Building Climate Control with Seasonal Energy Storage

Simon O. Weber,Marius Oei,Marc Linder,Michael Böhm,Phillip Leistner,Oliver Sawodny

- Two concepts for model predictive control of a building system with seasonal thermochemical energy storage are presented

- The control concepts distinguish in the way a superior optimal generation scheduling trajectory is followed: objective or constraint-based reference tracking

- The impacts of different building envelopes, heat supply configurations, electricity price fluctuation ranges, control parameter sensitivity and conceptual control robustness with respect to different weather and electricity price data are also analysed

- One control approach enables best annual operation costs and does not require a higher-level scheduling hierarchy

Model Predictive Approaches for Cost-Efficient Building Climate Control with Seasonal Energy Storage

Simon O. Weber[a,*], Marius Oei[b], Marc Linder[c], Michael Böhm[b], Phillip Leistner[a] and Oliver Sawodny[b]

[a]*Institute for Acoustics and Building Physics, University of Stuttgart, Pfaffenwaldring 7, 70569 Stuttgart, Germany*
[b]*Institute for System Dynamics, University of Stuttgart, Waldburgstraße 19, 70563 Stuttgart, Germany*
[c]*Institute of Engineering Thermodynamics, German Aerospace Center, Pfaffenwaldring 38–40, 70569 Stuttgart, Germany*

ABSTRACT

In order to store the surplus summer electrical energy supply and satisfy the winter heat demand, a seasonal energy storage system with a high capacity is required. The aim of this work is the control integration of a novel thermochemical seasonal energy storage concept into a building energy system.

In this work a state based model is developed consisting of a building, a water buffer and a heat supply. In order to elaborate the effects of long-term storage long-term weather forecasts are applied and the heat supply is varied. Since public weather forecasts are reliable in the time range of several days, test reference year data are used to approximate the weather forecast beyond the public forecast period.

On this basis, two Model Predictive Control (MPC) concepts are designed to efficiently operate the system over one year. The hierarchy is comprised of a superordinate optimal generation scheduling (OGS) and a subordinate MPC. The concepts follow the scheduled long-term lime storage trajectory and realise possible short-term yields based on the current public forecast. The trajectory tracking is formulated either in the objective function or the constraints.

The integration of the novel lime storage module into the heat supply of a building allows a reduction of operating costs of 18 % in the realistic scenario and up to 80 % in case of highly fluctuating electricity prices. This reduction potential is fully exploited by the developed control approaches, but it is very sensitive to the change of the controller parameters, the fluctuation of the electricity price and the weather data. Moreover, by applying the best possible control approach and parameter set, the higher-level scheduling hierarchy could be avoided.

1. Introduction

Climate change is one of the biggest challenges of modern human history. For this reason, 195 countries joined together in 2016 aiming to limit global warming to at most 2 °C compared with the pre-industrial age [1]. The German Federal Government has also joined the Paris Agreement and laid down goals of greenhouse gases reduction by 65 % and a share of renewable energies of 65 % until 2030. The introduction of a minimum price for CO_2 and the phasing out of coal-fired power generation by 2038 should initiate complete climate neutrality by 2045 [2]. According to a recent study, 53.2 % of the final energy consumption in Germany is used for space heating, hot water supply and process heat [3]. Furthermore, the increasing share of renewable energies causes a growing fluctuation of energy production [4]. Energy storage systems separate the generation and consumption of energy and thus create flexibility in the energy system. The use of energy storage systems for the heating of buildings thus has enormous potential to help achieve climate neutrality.

There are many suitable materials for thermal energy storage. The latest comprehensive analysis and comparison

can be found in the following review [5]. They can be categorised into sensible (hot water), latent (phase change materials) and thermochemical (sorption or chemical reaction based) storage materials. "Thermochemical materials have the advantage of high heat storage density, a significant temperature increase, and the possibility of storing the reactants (sorbent and sorbate) at ambient temperature and with no self-discharge" [6]. Compared to latent thermal energy storage, thermochemical materials have more than twice the energy density and up to 10 times the energy density of sensible energy storage materials. The storage technology considered in this work is based on the material cycle $Ca(OH)_2$ (slaked lime) / CaO (burnt lime). The material is promising due to its high energy density as well as low cost of 0.15 € per kWh of storage capacity [7]. To fully utilise the potential of thermochemical storage on the seasonal scale, the material should not only go through a single cycle (summer/winter), but also take advantage of short-term fluctuations in ambient conditions for intermediate loading. This task requires a capable trajectory planning and model based control approach. While a rule-based approach can very easily follow a previously calculated lime storage trajectory, it cannot identify the advantages and disadvantages of an anticipated storage due to low electricity prices and high heat demand. For this purpose, model predictive control schemes have to be established.

Model predictive control is a well-studied control con-

*Corresponding author

✉ simon.weber@iabp.uni-stuttgart.de (S.O. Weber)
🌐 www.iabp.uni-stuttgart.de (S.O. Weber)
ORCID(s): 0000-0002-6268-8547 (S.O. Weber); 0000-0003-3077-4245
(M. Oei); 0000-0003-2218-5301 (M. Linder); 0000-0002-6290-5783 (M. Böhm); 0000-0002-6910-2473 (O. Sawodny)

Nomenclature

Abbreviations

AOC	annual operation cost
BRCM	Building-Resistance-Capacitance-Modelling
COP	coefficient of performance
CORT	constraint-based reference tracking
EPS	expanded polystyrene
HP	pure heat pump heat supply configuration
LS	pure lime storage heat supply configuration
LSHP	hybrid heat supply configuration
MDF	medium density fiberboard
MPC	model predicitve control
OGS	optimal generation scheduling
ORT	objective-based reference tracking
SHGC	solar heat gain coefficient
TRY	test reference year

Chemical Formulas

$Ca(OH)_2$	calcium hydroxide
CaO	calcium oxide
H_2O	water

Latin Symbols

α	heat transfer coefficient ($W\,m^{-2}\,K$)
$\dot{m}$	mass flow ($kg\,s^{-1}$)
$\dot{Q}$	heat flow (W)
γ	solar absorption factor (−)
λ	heat conduction coefficient ($W\,m^{-1}\,K$)
ρ	density ($kg\,m^{-3}$)
ϑ	temperature (°C)
ζ, ξ	efficiency parameters lime storage ()
A	area (m^2)
A, B_u, B_v	state, input, disturbance matrix
B_{xu}, B_{vu}	state-input, disturbance-input bilinearity matrix
c_p	specific heat capacity at constant pressure ($J\,kg^{-1}\,K$)
H	enthalpy (J)
I	solar radiation power on facade ($W\,m^{-2}$)

K	constant model value
L	stage cost (EUR)
P	electrical power (W)
$rdev$	relative deviation (−)
T	temperature (K)
U	heat transmission coefficient ($W\,m^{-2}\,K$)
V	volume (L)
w_B	mass based energy density quicklime ($kJ\,kg^{-1}$)
w_C	volumetric energy density water ($kJ\,L^{-1}$)
x, u, v	state, input, disturbance vector

Subscripts

16	2016
ACR	air change rate
AMB	ambient
B	blind
BD	building
BS	buffer storage
by	base year
CH	chiller
ch	charging
cl,vl	constant loss, variable loss
cy	current year
dc	discharging
DHW	domestic hot water
E,N,S,W	east, north, south, west
EP	electricity price
EW	external wall
IG	internal gain
IW	inner wall
LS	lime storage
OP	occupancy
RD	radiatior
Z	zone

cept for building energy systems in general. It belongs to the optimal control methods where the system inputs are step-wise calculated by optimizing an objective function under constraints. A recent review about MPC within the building sector is supplied by Drgoňa et al [8]. Both the simulative [9, 10, 11, 12] and the experimental implementation of MPC [13, 14] have been a focus of recent research. In one practical MPC implementation, a reduction of energy consumption by up to 29 % as well as better comfort compared to an operation mode by heating curve could be achieved [14]. Finck et al. applied MPC to a system consisting of a building, heat pump, and thermal energy storage and found that the sensible hot water storage tank offers a higher potential to provide short-term (i. e. intra-day) energy flexibility when compared to a thermochemical storage [9]. Previously, the same research group carried out a single cost optimisation and considered the operating costs of different heat supply configurations over an entire year [15] for test ref-

erence year data (TRY). In combination with a heat pump, a solar-powered phase change or thermochemical storage tank reduced the operating costs by 13 % and 8 %, respectively, compared to a configuration without storage. Research has also been conducted on the control of long-term thermal storage systems based on insulated water tanks. Xu et al. [11] focus on the detailed dynamics description of solar heated borehole storage with a prediction horizon of 5 days whereas Jonin et al. [12] focus on the inertial behaviour of different layers within a seasonal solar heated water tank over a whole year.

Hierarchical approaches to model predictive control have been developed for microgrids [16] and building energy systems [13, 10, 17]. They have in common that they divide the calculation into two hierarchies. In the long-term prediction horizon mostly the system states, for example the battery state of charge and the hydrogen level [16], the PCM enthalpy [10] are considered. For this purpose, a predic-
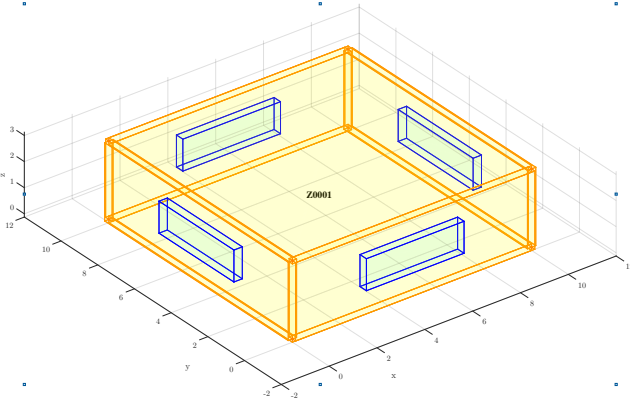
tion horizon between 7 hours [17] and 3 days [16] is used. The objective is defined as pure operating cost [10, 17] or scenario-weighted operating cost [16]. In the short-term prediction horizon, the calculated states and inputs are more or less followed. In the work of Touretzky et al.[10] a pure tracking objective and a pure economic objective are compared with each other. In contrast, the objective in the work [16] consists of empirically weighted power variables, power rates, and tracking parts of the storage states. The short-term prediction horizon is between ten seconds [16] and one hour [13].

Within this literature review, none of the considered works has integrated a seasonal thermochemical energy storage into a building system from a control perspective. Accordingly, two hierarchical MPC concepts are established, which forecast more than one year forward on the long-term prediction level. Furthermore, for the short-term prediction level it has not yet been investigated whether it is better to formulate a weighted approach between economic and tracking objective and common constraints or a economic objective and trajectory tracking within the constraints.

Based on the current state of research, the following hypotheses are formulated:

1. By integrating a thermochemical energy storage system into the building system, the operating cost and energy consumption of the overall system can be reduced.

2. The cost saving by integrating the seasonal energy storage system depends on the fluctuation of electricity price.

3. The system of building and seasonal energy storage can be efficiently controlled by integrating the trajectory tracking into the objective function instead of defining it as a constraint.

4. To the extent that the trajectory tracking is integrated into the objective criterion, there is an optimal weighting between the short-term energy consumption in the system and the long-term energy storage.

5. To successfully operate a seasonal energy storage system, a prediction horizon greater than that of public weather forecasts must be applied.

6. The energy consumption of a building depends on the building envelope and is higher for lightweight constructions than for standard façade constructions.

The last hypothesis basically arises within the Collaborative Research Centre SFB1244 and is investigated as a secondary hypothesis. To clarify these hypotheses, a simple model of a thermochemical energy storage system and a water buffer storage system is set up and connected to the validated model of a building. Three different heat supply configurations are compared to investigate the effects of long-term storage. In the HP configuration, heat is provided exclusively by a heat pump. In the pure lime storage configuration LS, the heat is provided exclusively by the lime storage module. The hybrid configuration combines the heat pump with the lime storage module. Consequently, two MPC concepts are set up based on a two-layer hierarchical approach. In the long-term prediction level optimal lime storage trajectories are calculated

Figure 1: Flow diagram of the total energy system. Heat supply configuration *HP* blue, *LS* orange, *LSHP* in green frame.

based on TRY weather data and averaged electricity price data. The two approaches differ in the short-term prediction horizon as one considers the trajectory tracking in the objective function and the other considers it in the constraint. All approaches aim to minimise the yearly operating cost while ensuring comfortable built environment. An investigation on robustness of the best control approach is conducted.

Sections 2 to 3 present the system model and introduce two distinct control concepts. The results of the electricity price fluctuation, different heating supply configurations and control parameter variation are presented and discussed in section 4. The work is summarised and open questions, as well as further research topics, are discussed in section 5.

2. System Model

In this work, an energy system is considered that contains a building, a water buffer storage and a heat supply. Three different configurations for the heat supply are investigated. The heat supply configurations *HP*, *LS*, *LSHP* are depicted in fig. 1. The total system dynamics $\dot{x} = (\dot{x}_{BD}, \dot{x}_{BS}, \dot{x}_{LS})^T$ is composed of the building, buffer storage and lime storage dynamics, respectively.

2.1. Building System

The thermal model of the building is created using the validated Building-Resistance-Capacitance-Modelling (BRCM) toolbox [18]. "Over the five-day period, the zone air temperature difference was within 0.5 °C" difference to the zone temperature predicted by EnergyPlus [19]. Despite being less accurate for times with high solar radiation, this modelling approach has the advantage of providing access to gradients and thus simplifying convex optimisation [19].

The building zone is designed as one floor of an office

Figure 2: Thermal zone as one floor of an office building.

Table 1
Constructions of the building walls.

Type	Wall	Material	Thickness [cm]
Heavy	Internal walls	M1	25
	External walls	M2,M3,M1	2,14,16
Light	Internal walls	M2	12.5
	External walls	M2,M3,M2	2,14,2

Table 2
Material properties of the building walls. Source [21, 22]

Name	Identifier	c_p[J/kgK]	λ[W/mK]	ρ[kg/m³]
Concrete	M1	1000	1.65	2200
MDF	M2	1700	0.10	400
EPS	M3	1210	0.03	10

building, with a floor area of $100\,\mathrm{m}^2$ and a ceiling height of 3 m as depicted in fig. 2. The heat exchange of the floor downwards and the ceiling upwards is considered adiabatic. The facades have the ambient temperature as outside boundary condition. The inner and outer wall combined radiative and convective heat transfer coefficients were taken from the EN ISO 6946 standard [20] with α_i=7.7 W m^{-2} K^{-1} and α_e=25 W m^{-2} K^{-1}, respectively. Since resource-efficient ultra-lightweight construction methods are being researched in the Collaborative Research Centre SFB1244, this work compares the system efficiency of a lightweight and heavyweight building envelope construction in addition to the concepts for seasonal energy storage control. The employed heavy and light envelope construction and material properties are according to table 1 and table 2. Every external wall on each facade side consists of three layers. The ceiling and the floor are the internal walls and consist of one layer.

Each external wall contains a window of the same type. Its window and frame area as well as the combined heat transfer coefficient of frame and glass U and the Solar Heat Gain Coefficient (SHGC) were set according to table 3.

The building thermal model is influenced by external heat flows. These are due to external disturbances such as outdoor air temperature and solar irradiation or by internal

Table 3
Specification parameter of the building windows.

$A_{transparent}$[m²]	A_{frame}[m²]	U [W/m²K]	f_{SHGC} [$-$]
6	2	1.3	0.6

gains. Heat flows caused by internal gains such as heat generated by occupants, lighting, and computers, directly impact the room temperature and are scaled with the occupancy density. The total daily internal gain heat flux is $\dot{Q}_{IG}$=102 W h m^{-2} d, equivalent 8 occupants in the office with additional appliances, computers and lightning according to the standards [23, 24].

The air handling unit applies further heat flows directly to the zone. It provides the heating and cooling power to control the temperature of the room and ensures sufficient supply of fresh air to occupants.

The solar radiation on the outer walls is multiplied with the absorption factor (γ=0.5) to yield the radiant heat flow. The solar radiation part that passes through the window glazing and is converted into heat is described by the solar heat gain coefficient f_{SGHC}. The convective part of the transmitted heat acts directly on the zone, which is described by secondary heat gain coefficient (f_{secHG}=0.1), the radiative part is distributed equally among the wall elements.

After defining the input files, the BRCM toolbox provides the building model matrices. Corresponding to the procedure in VDI 6007-1 [25], the order of the detailed building model is now reduced. To this end, the energy balance of the ceiling and the floor are merged into one inner wall and all layers of the outer walls with the same structure into one layer. The reduced building model eq. (1) is bilinear due to the interactions between the blinds and solar radiation, and between air exchange rate and the zone and ambient temperature. The state vector eq. (2) of the reduced building model x_{BD} now includes only the temperature of the zone T_Z, the inner wall T_{IW} and each layer of the external wall $T_{EW,j}$. The building's manipulated variables u_{BD} eq. (3) are the blind positions in each facade's window $u_{B,i}$, the air exchange rate u_{ACR} as well as the heating and cooling power $\dot{Q}_{RD}, \dot{Q}_{CH}$. The disturbance inputs v as well as the state and input constraints are given in the section 2.4 and section 2.5.

$$\dot{x}_{BD} = A_{BD}x_{BD} + B_{u,BD}u_{BD} + B_{v,BD}v$$
$$+ \sum_{i}^{dim_u}(B_{xu,i}x + B_{vu,i}v)u_i \quad (1)$$

$$x_{BD} = (T_Z, T_{IW}, T_{EW,1}, T_{EW,2}, T_{EW,3})^T \quad (2)$$

$$u_{BD} = (u_{B,E}, u_{B,N}, u_{B,S}, u_{B,W}, u_{ACR}, \dot{Q}_{CH}, \dot{Q}_{RD})^T \quad (3)$$

2.2. Buffer Storage Tank

The model for the water buffer tank eq. (4) was derived from the enthalpy balance assuming isothermal and spatially homogeneous conditions at storage temperature ϑ_{BS}=55 °C.

It is supplied by the heat pump $\dot{Q}_{HP}$, the heat flow during lime storage charging $\dot{Q}_{LS,ch}$ and discharging $\dot{Q}_{LS,dc}$. The last two heat flow parts are derived in the next section 2.3. The COP of the heat pump and chiller is assumed to be constant at COP_{HP}=4.0, COP_{CH}=7.1, respectively, according to the *Bosch Climate 5000 RAC 5.3* [26] specification. The required radiator heat $\dot{Q}_{RD}$ and domestic hot water supply $\dot{Q}_{DHW}$ as well as heat losses reduce the energy in the storage tank. The occupancy dependant domestic hot water heat flow was set to $\dot{Q}_{DHW}$=506 Wv_{OP} according to the standards [24, 27]. Constant heat losses $\dot{Q}_{BS,cl}$ occur at the walls of the storage tank and hot water supply pipes according to standards [24, 27] and are set to $\dot{Q}_{BS,cl}$=579 W. Variable heat loss $\dot{Q}_{BS,vl}$ is enabled by draining water from the tank, as suggested by Schmidt [28]. The current stored volume of water eq. (5) is given by the volume-related energy content at storage temperature w_C=227.0 kJ L^{-1}. Equations (6) to (9) describe the open entries of the water buffer model eq. (4).

$$\dot{x}_{BS} = B_{u,BS}u_{BS} + B_{v,BS}v_{OP} + K_{BS} \qquad (4)$$
$$x_{BS} = V_{BS} \qquad (5)$$
$$u_{BS} = (\dot{Q}_{RD}, \dot{Q}_{BS,vl}, \dot{Q}_{HP}, P_{LS,ch}, \dot{m}_{LS,dc})^T \qquad (6)$$
$$B_{u,BS} = \begin{pmatrix} -1 & -1 & 1 & \zeta & w_B \end{pmatrix}/w_C \qquad (7)$$
$$B_{v,BS} = -506\,\text{W}/w_C \qquad (8)$$
$$K_{BS} = -\dot{Q}_{BS,cl}/w_C \qquad (9)$$

2.3. Lime Storage System

The concept of the novel lime storage module and the system equations were taken from the publication by Schmidt [28]. For a detailed insight and their in-depth derivation of the concept, please refer to this publication. The plow share mixer generates a mechanically assisted fluidized bed. This reactor concept allows a high energy input within a compact design and is well suited for building applications. Within the Collaborative Research Centre SFB1244 this concept is currently implemented into the demonstrator high-rise building. In principle, either surplus photovoltaic electricity in summer or time-independent low-cost electricity is stored within the reaction enthalpy of the material combination calcium hydroxide (slaked lime Ca(OH)$_2$) / calcium oxide (burnt lime CaO). However, a photovoltaic model is not included in this work. The thermochemical energy storage can be assumed to be loss-free over a seasonal period. During the charging cycle (ch), slaked lime reacts at temperatures of 450 °C to form quicklime eq. (10). The enthalpy of condensation of the water vapour released in this process as well as a part of the sensible energy could be directly used for space conditioning. In the discharge cycle (dc) eq. (11) quicklime reacts with water back to slaked lime. The energy released in this process is likewise used for space conditioning. For simplicity, the heat transfer at the heat exchanger is assumed to be lossless.

$$\text{Ca(OH)}_2 + 104.4\,{}^{\text{kJ}}\!/_{\text{mol}} \xrightarrow{\text{ch}} \text{CaO} + \text{H}_2\text{O}_{(g)} \qquad (10)$$

$$\text{Ca(OH)}_2 + 65.1\,{}^{\text{kJ}}\!/_{\text{mol}} \xleftarrow{\text{dc}} \text{CaO} + \text{H}_2\text{O}_{(l)} \qquad (11)$$
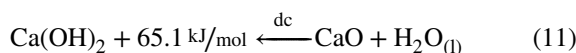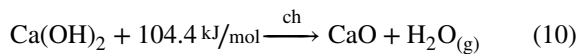
The lime storage model is derived from the isothermal energy balance eq. (12) on the quicklime component m_{LS} with the given energy density w_B=1162.5 kJ kg^{-1} according to Schmidt et al. [28]. They propose that 58 % of the electrical power input is available for long-term storage eq. (13) and 42 % for direct space conditioning eq. (14). The heat flow released during discharge $\dot{H}_{dc}$ eq. (15) acts lossless on the water buffer tank. Equations (16) to (18) describe the total subsystem model, the subsystem state as mass of lime and the subsystem inputs, respectively.

$$\dot{H}_{LS} = \dot{H}_{ch} - \dot{H}_{dc} \qquad (12)$$
$$\dot{H}_{ch} = \xi P_{LS,ch} \qquad \xi = 0.58 \qquad (13)$$
$$\dot{Q}_{LS,ch} = \zeta P_{LS,ch} \qquad \zeta = 0.42 \qquad (14)$$
$$\dot{Q}_{LS,dc} = \dot{H}_{dc} = w_B \dot{m}_{LS,dc} \qquad (15)$$
$$\dot{x}_{LS} = \left(\xi/w_B \quad -1\right) u_{LS} \qquad (16)$$
$$x_{LS} = m_{LS} \qquad (17)$$
$$u_{LS} = (P_{LS,ch}, \dot{m}_{LS,dc})^T \qquad (18)$$

2.4. Disturbances

The system disturbance

$$v = (v_{OP}, T_{AMB}, I_E, I_N, I_S, I_W)^T \qquad (19)$$

is composed of the current occupancy density v_{OP} of the office's zone, the ambient temperature T_{AMB}, and the vertical radiation intensities I_i on each facade. The disturbance input v_{EP} is the hourly electricity price and only influences the objective function.

The occupancy density profile v_{OP} is equal to that in Finck's work [29] and applied for each weekday of the year without holidays. The weather data stems from the European Union PVGIS database [30] at the SFB1244 high rise building demonstrator location (N 48.749°, E 9.112°) on the University of Stuttgart campus. The electricity costs v_{EP} are spot market prices accessible via the online platform of the German Federal Network Agency [31]. The mean value of the electricity price was adjusted such that the relative standard deviation related to the mean value matches a defined value. This adjustment is justified in more detail in the results section 4.1. The disturbance inputs of the so called base year were created from typical meteorological weather data (2005–2016) and hourly averaged electricity prices (2015–2018). The occupancy density data were not averaged and the same profile was used for both the base year and the current year. The current year weather and electricity price data were single year data of the year 2015 and 2016. Figure 3 depicts the ambient air temperature and electricity price for 2016.

2.5. Constraints

The system variables are subject to time variant constraints. Within the presence of at least one person the room temperature must be between 21 °C and 24 °C according to the standard [24]. Otherwise the constraint is relaxed to 17 °C and 28 °C. The buffer storage tank has a capacity
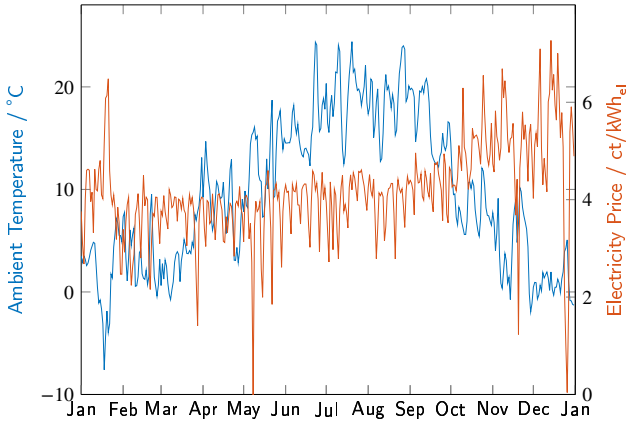
Figure 3: Ambient temperature and daily mean electricity price for the current year 2016.

of 1000 L whereas no upper limit is imposed on the lime storage tank.

$$\mathbb{X}(t) := \left\{ x \in \mathbb{R}^7 : \begin{matrix} \vartheta_Z & \in \begin{cases} [21;24] & v_{OP}(t) > 0 \\ [17;28] & \text{else} \end{cases} \\ V_{BS} \in [0;1000] \\ m_{LS} \geq 0 \end{matrix} \right\} \quad (20)$$

The blind position values are continuous within zero (fully closed) and one (fully open). Based on the standard [24], the air exchange rate is constrained by $2\,h^{-1}$ to $3\,h^{-1}$, if a person is in the office. The air exchange rate may be within $0\,h^{-1}$ to $6\,h^{-1}$ outside the operating hours, to enable efficient overnight cooling. The upper bounds of the chiller, radiator, and heat pump power are set according to the specification data sheet of the Bosch Climate 5000 RAC. The power input to the lime reactor is limited to 10 kW. The variable heat loss from the buffer storage $\dot{Q}_{BS,vl}$ as well as the discharging quicklime mass flow $\dot{m}_{LS,dc}$ must naturally be greater than zero.

$$\mathbb{U}(t) := \left\{ u \in \mathbb{R}^{11} : \begin{matrix} u_{B,E} & \in [0;1] \\ u_{B,N} & \in [0;1] \\ u_{B,S} & \in [0;1] \\ u_{B,W} & \in [0;1] \\ u_{ACR} & \in \begin{cases} [2;3] & v_{OP}(t) > 0 \\ [0;6] & \text{else} \end{cases} \\ \dot{Q}_{RD} & \in [0;4100] \\ \dot{Q}_{CH} & \in [0;5200] \\ \dot{m}_{BS,vl} & \geq 0 \\ \dot{Q}_{HP} & \in [0;4100] \\ P_{LS,ch} & \in [0;10000] \\ \dot{m}_{LS,dc} & \geq 0 \end{matrix} \right\} \quad (21)$$

2.6. Discretisation

The continuous dynamic model equations are discretised, analogue to the work [18], using the exact discretisation of the state and zero-order hold assumption for the manipulated and disturbance input at an interval length of $dT = 1\,\text{h}$.

3. Model Predictive Control Concepts

All model predictive control concepts are hierarchically integrated into the plant management layer. Thus, they specify setpoints for the control loops at the automation layer, as depicted in the review diagram [8, fig. 11]. The control approaches provide a two level hierarchy consisting of a superordinate whole-year optimal generation scheduling (OGS) and subordinate dynamic MPC. The OGS not only passes the reference trajectory to the dynamic MPC but also serves to analyse the heat supply configurations.

The calculations of OGS and MPC simulations were carried out with the algorithmic differentiation Matlab toolbox CasADi using the interior point optimization implementation IPOPT [32]. The calculations where carried out on a Lenovo P14s with AMD Ryzen 7 PRO 5850U and 32.0 GB RAM. The long-term prediction is calculated with a time step of 1 h, a time horizon of 365 days and is not updated after a certain control horizon as usual, because the computational effort would be excessive and the annual lime storage curve would remain the same due to the periodicity of the weather data. The MPC approaches are applied with a time step of 1 h, a control horizon of 60 h and a time horizon of 5 days.

3.1. Optimal Generation Scheduling

The optimal lime storage trajectory is previously determined by the OGS algorithm eq. (23) based on the chosen disturbance input. It is the result of a single optimisation of the annual operating costs (AOC), while satisfying the aforementioned state and input constraints and the provided discretised system model. The second condition reflects the periodicity of the disturbance data. The stage costs $L(k)$ eq. (22) are non-linear and result from the AOC. The AOC are determined by the current electricity price as well as the electrical power for cooling, the heat pump, and the charging power of the lime storage module.

$$L(k) = v_{EP}(k) \left(\frac{\dot{Q}_{CH}(k)}{\text{COP}_{CH}} + \frac{\dot{Q}_{HP}(k)}{\text{COP}_{HP}} + P_{LS,ch}(k) \right) \quad (22)$$

$$\begin{aligned}
\min_u \quad & \sum_{k=0}^{n-1} L_{by}(k)dT \\
\text{s.t.} \quad & n = 8760, \\
& x(0) = x(n), \\
& x(k+1) = f(x(k), u(k), v_{by}(k)) \quad \forall k \in [0, n-1], \\
& u(k) \in \mathbb{U}(k) \quad \forall k \in [0, n-1], \\
& x(k) \in \mathbb{X}(k) \quad \forall k \in [0, n]
\end{aligned} \quad (23)$$

3.2. Dynamic MPC

The goal of the dynamic MPC approaches is an optimal path following of a long-term reference storage level trajectory while reacting to short-term conditions in the current year. The basic assumption behind both concepts is
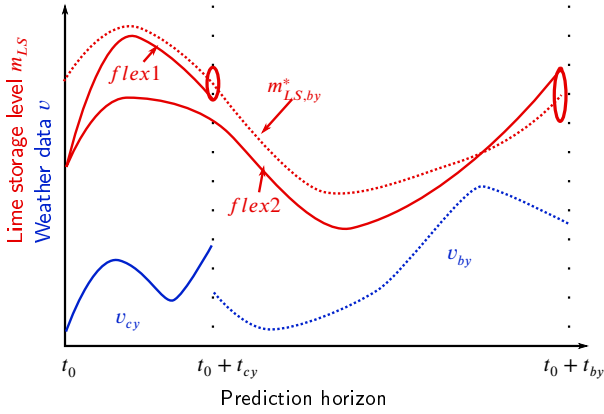
Figure 4: Summarising illustration of proposed control approaches and disturbance data approximation.

that the efficient operation of a seasonal energy storage system requires a larger horizon than that of public weather forecasts. Therefore, the planning horizon is divided into two time periods, the control and restoration period. Figure 4 illustrates the basic principle. In the control period $\tau \in [t_0, t_0 + t_{cy}]$, the current public weather, occupancy, and electricity price forecast v_{cy} is applied. In the restoration period $\tau \in [t_0 + t_{cy}, t_0 + t_{cy} + t_{by}]$, the weather data of the so-called base year are used. The generation of this disturbance data was explained in section 2.4. The control concepts differ in the formulation of the objective and constraints in the restoration period. By definition, within the second period the lime storage mass at its end must follow the OGS reference more or less flexibly.

The control concepts are analysed for various values of their flexibility parameters as well as the system configurations LS and $LSHP$. Thus, the central criterion for comparison is the relative deviation $rdev$ of the annual operation costs of the MPC controller compared to the best possible trajectory OGS_{16}. This trajectory is the result of the OGS algorithm not using the base year but the single year 2016 disturbance data.

$$rdev = \frac{AOC - AOC[OGS_{16}]}{AOC[OGS_{16}]}. \tag{24}$$

Objective-based reference tracking (ORT)
In this approach eq. (25) the objective function consists of a weighted mixture between the economic cost within the current year prediction horizon and the trajectory tracking. Only the amount of lime stored at the end of the current year prediction horizon is tracked. This approach was derived from the fact that possible deviations of the lime storage mass from the reference at the end of the current year prediction horizon should decrease linearly towards the end of the base year prediction horizon. Further details and the derivation of this control concept are presented in the underlying reference work [33]. The control parameters varied are

the prefactor p and power m.

$$\min_u \sum_{k=0}^{n_1-1} L(k)dT + \left(p(m_{LS,by}(n_1) - m_{LS}(n_1)) \right)^m$$

s.t.

$$
\begin{aligned}
n_1 &= \frac{t_{cy}}{dT} = 120, \\
x(0) &= x(t_0), \\
x(k+1) &= f(x(k), u(k), v_{cy}(k)) \quad &\forall k \in [0, n_1 - 1], \\
u(k) &\in \mathbb{U}(k) \quad &\forall k \in [0, n_1 - 1], \\
x(k) &\in \mathbb{X}(k) \quad &\forall k \in [0, n_1]
\end{aligned}
\tag{25}
$$

Constraint-based reference tracking (CORT)
The objective of the second MPC approach includes the economic costs within both the control and restoration period (variables marked with tilde). Accordingly, it is a purely economic objective function. In contrast to the first approach the states, inputs and constraints within the restoration period are explicitly formulated. The trajectory tracking is fulfilled as a lower bounded final state constraint. The ϵ factor shifts the lower limit of the lime storage capacity to the end of the restoration phase and ensures minimum build-up. The control concept is also analysed for various values of the flexibility parameter sets (ϵ, t_{by}) as well as the system configurations LS and $LSHP$.

$$\min_{u, \tilde{u}} \sum_{k=0}^{n_1-1} L(k)dT + \sum_{l=0}^{n_2-1} \tilde{L}_{by}(l)dT$$

s.t.

$$
\begin{aligned}
n_1 &= \frac{t_{cy}}{dT} = 120, \\
x(0) &= x(t_0), \\
x(k+1) &= f(x(k), u(k), v_{cy}(k)) \quad &\forall k \in [0, n_1 - 1], \\
u(k) &\in \mathbb{U}(k) \quad &\forall k \in [0, n_1 - 1], \\
x(k) &\in \mathbb{X}(k) \quad &\forall k \in [0, n_1], \\
n_2 &= \frac{t_{by}}{dT}, \\
\tilde{x}(0) &= x(n_1), \\
\tilde{x}(l+1) &= f(\tilde{x}(l), \tilde{u}(l), v_{by}(l)) \quad &\forall l \in [0, n_2 - 1], \\
\tilde{u}(l) &\in \mathbb{U}(l) \quad &\forall l \in [0, n_2 - 1], \\
\tilde{x}(l) &\in \mathbb{X}(l) \quad &\forall l \in [0, n_2], \\
\tilde{m}_{LS}(n_2) &\geq \epsilon m_{LS,by}(n_2)
\end{aligned}
\tag{26}
$$

4. Results & Discussion

The computational time of annual simulation of the ORT approach does not strongly depend on the control parameter values and is about two minutes. In contrast, one annual simulation with the CORT approach took between two minutes and 25 h ($LSHP$) or 16 h (LS), depending on the base

year prediction horizon. The differences in computing time between the configurations *LS* and *LSHP* are due to the additional heat pump input. This reveals that for general problems that require a much more detailed description of the energy system and additional control inputs, a much longer calculation time is to be expected. To reduce the solution complexity, model reduction procedures like Krylov subspace methods or the addition of another control hierarchy level are sensible approaches.

The focus of the subsections is as follows: In section 4.1, the impact of electricity price fluctuation on the cost benefit of the lime storage module is examined. In section 4.2, the heat supply configurations are analysed for their impact on the overall system. In sections 4.3 to 4.4, we examine the sensitivity of the controller parameters to the annual performance for both control approaches. In addition, in section 4.3 the suitability of the base year lime storage trajectory is evaluated. Finally, in section 4.5, the robustness of the ORT approach to different weather data and electricity price signals is investigated.

4.1. Analysis on the electricity price fluctuation

At the beginning of the study, it was found that the fluctuation range of the electricity price has a decisive influence on the benefits provided by the lime storage module. For this purpose, the mean value of the 2016 spot market electricity price including taxes and levies was varied and OGS simulations of the system with different heat supply configurations were performed. Figure 5 shows the cost savings of the configurations with the lime storage module compared to the heat pump configuration against the relative fluctuation range *rstd* of the electricity price signal. This is defined by the quotient of the annual standard deviation by the mean value of the electricity price signal. Accordingly, the savings and the maximum stored lime quantity increase rapidly from a relative fluctuation range of 30 %. Negative values of cost reduction mean annual operating cost increase and vice versa. Accordingly, the heat supply configuration *LS* is in neither case more economical than the heat pump configuration. However, it will continue to be pursued, as it probably offers advantages in the consideration of life cycle costs.

Including taxes and levies, the relative fluctuation range of the electricity price for industrial customers in Germany is approx. 6-9 % apart from 2021. Figure 6 therefore depicts the relative fluctuation range of the electricity price including taxes and levies of other European countries. The standard deviation of the electricity signals were taken from the data of the Federal Network Agency [31] and the annual mean price with taxes and levies from EUROSTAT [34] data. It is shown that seasonal energy storage with lime is better suited in Eastern European countries due to their lower tax burden resulting in higher relative fluctuation range *rstd*. In addition, a recent publication [4] concludes that the relative fluctuation range of the electricity price in Germany will increase by 20 % to 54 % by 2030, depending on the scenario. Applied to the high relative fluctuation range of the electricity signal in other European countries, a value of 30 %
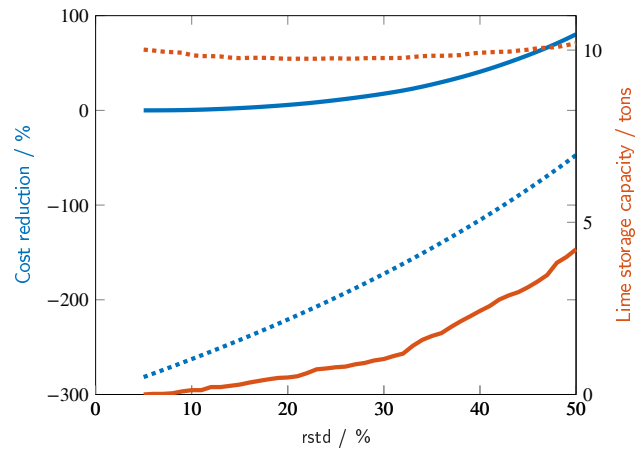
Figure 5: Cost reduction compared to *HP* configuration AOC and maximum lime storage capacity due to hybrid lime storage *LSHP* (solid) or pure lime storage configuration *LS* (dashed) against the relative fluctuation range *rstd*.
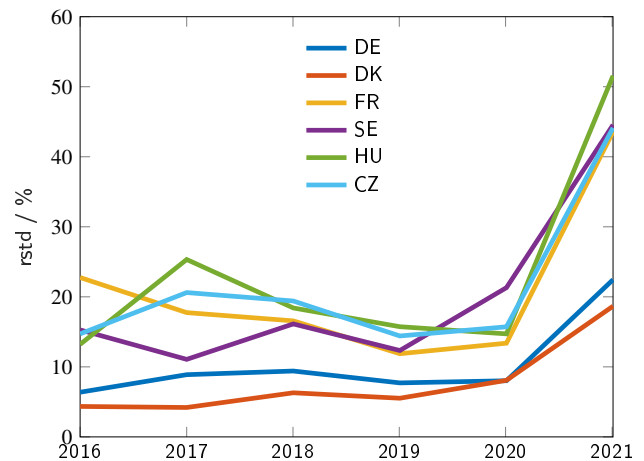

Figure 6: Relative fluctuation range of the electricity spot market price for different European countries.

seems very likely and represents a significantly beneficial setting for the hybrid configuration *LSHP*. Accordingly, all electricity price signals used were raised upwards by a constant value such that the specified relative fluctuation range of 30 % is maintained. These results support the hypothesis 2 that the fluctuation of the electricity price in particular the fluctuation range is crucial to successfully operate a seasonal energy storage system.

Figure 7 depicts the relative deviation of the electricity price during charging from the annual mean electricity price against the relative fluctuation range. The solid lines are those deviations of the mean charging prices (frequent prices) and the dashed lines are the mean plus standard deviation prices (seldom prices). Compared to the lower limit of the relative electricity price fluctuation (black line), the lime storage charging starts significantly below it. As the electricity price fluctuation increases, the price during charging increases. Probably, more lime cannot be stored to the same extent in the narrow time range of increasingly sharp price
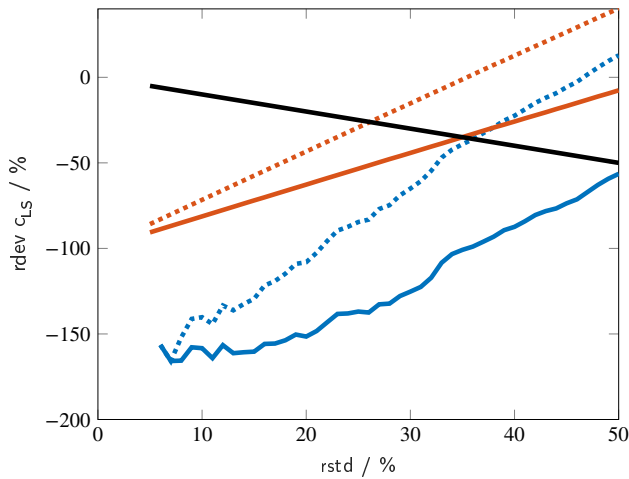
Figure 7: Relative deviation of the frequent (solid) and seldom (dashed) electricity price during storage loading to the annual mean electricity price versus the relative fluctuation range of the electricity price signal. The results are shown for the pure *LS* and hybrid *LSHP* configuration. Lower electricity price fluctuation range as black line.

Figure 8: Annual lime storage tank levels for the year 2016 with perfect prediction. The results are shown for the pure *LS* and hybrid *LSHP* configuration.

Table 4
Results of OGS simulations for varying heat supply configurations.

	Configuration	HP	LS	LSHP
light	AOC[€]	92	251	76
	AEU[kWh$_{el}$]	2749	10959	3305
	$\bar{c}_{HP}$[ct/kWh$_{el}$]	3.4	-	3.3
	$\bar{c}_{LS}$[ct/kWh$_{el}$]	-	2.3	-1.1
	$m_{S,B,max}$[kg]	-	9769	1030
heavy	AOC[€]	91	247	74
	AEU[kWh$_{el}$]	2718	10829	3287
	$\bar{c}_{HP}$[ct/kWh$_{el}$]	3.4	-	3.3
	$\bar{c}_{LS}$[ct/kWh$_{el}$]	-	2.3	-1.0
	$m_{S,B,max}$[kg]	-	9814	1117

dips. This should be addressed in future work. These results could lead to further stochastic control approaches.

4.2. Comparison of System Configurations

The OGS algorithm with 2016 data is employed to investigate the heat supply configurations under perfect prediction conditions. Table 4 depicts the resulting annual operation cost (AOC), annual energy usage (AEU) as well as the mean electricity price during heat pump or charging operation, $\bar{c}_{HP}$ and $\bar{c}_{LS}$ for a system configuration with light and heavy building respectively. Additionally, the maximum stored lime mass is evaluated as an indication for the required storage capacity.

As expected, the operating costs of the *LSHP* hybrid configuration with a light building construction are 17 % lower than those of the HP configuration and 70 % lower than those of the *LS* configuration. In contrast, the energy consumption is 20 % higher than that of the HP configuration and 70 % lower than that of the *LS* configuration. The higher energy

consumption of the lime storage module can be explained by the fact that the heat pump can provide more heat than the lime storage module from the electrical power due to its COP. It should be noted that the actual heat pump efficiency may be lower in the winter due to the lower ambient temperatures. Thus, the assumed constant heat pump COP of 4.0 is a rather generous estimate. However, the electricity price during charging of the lime storage tank within the hybrid configuration *LSHP* is significantly lower than the electricity price during heat pump operation, which leads to an overall reduced cost despite the increased energy consumption. It is even negative due to the applied relative fluctuation range. Referring to the first hypothesis, the operating costs are lower due to the integration of the seasonal lime storage, but the energy consumption is higher. The power consumption by the lime storage module can only be lower if the lime storage module equivalent to the heat pump could supply more reaction heat from the electrical energy. The use of high-temperature heat pumps may be an option here.

Furthermore, fig. 8 reveals the resulting lime storage trajectories of both heat supply configurations. In addition to the different maximum stored mass, there is also a lower fluctuation of the trajectory in the hybrid configuration. This is due to the rarer times at which lime is stored.

Within the configurations with heavy building envelope, the deviations are almost identical. There is very little difference between individual configurations with light and heavy building envelopes. The energy consumption with a heavy building envelope is about 1 % lower than with a light building envelope. These findings support the last study hypothesis to a very small degree. Compared to life cycle energy reductions, they could further favour ultra-lightweight construction methods and the goal of the Collaborative Research Centre SFB1244.
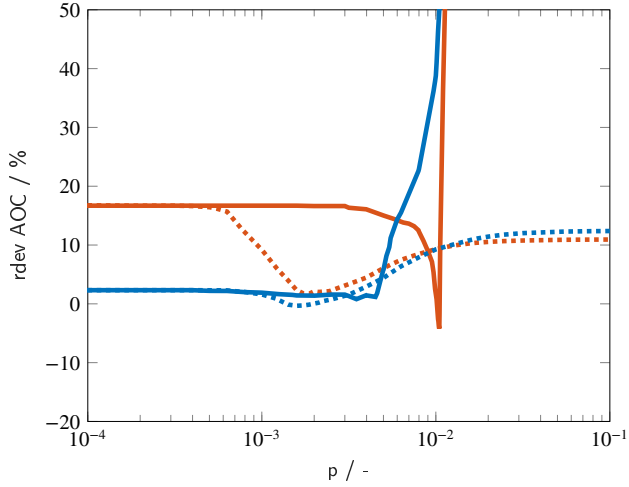
Figure 9: Results of the relative deviation $rdev$ for pure *LS* and hybrid *LSHP* configuration for exponents $m = 1$(solid), $m = 2$(dashed) and OGS weights p.

Table 5
Results of MPC ORT simulations relative deviation $rdev$ for parameter tuple $\{a, b\}$ and potency parameter m.

Conf	m	{1,0}	{0.6,0}	{0,0}	{0,1}
LS	1	-4.2	-4.2	-4.2	-4.2
LS	2	1.7	5.6	19.2	19.0
LSHP	1	0.8	0.8	0.8	0.8
LSHP	2	-0.3	1.1	2.3	1.2

4.3. Analysis of the ORT approach

The analysis on the first control approach is carried out by varying the prefactor p and the power m of the ORT objective. For a prefactor of $p=0$, the curves in fig. 9 align with each other depending on the configuration, since the influence of the tracking component in the objective function is withdrawn. Seasonal control does not play a role in this choice of the prefactor. In the negative prefactor range the deviation remains constant with single power $m=1$, since the changing of the sign of the tracking fraction leads to the direct minimization of lime storage mass. With a quadratic exponent $m=2$, the curves are the same as with a positive prefactor. With increasing prefactor, the deviations forms a flat minimum with the quadratic power and a sharp minimum with linear power at different minima. In the best case, the right choice of the prefactor activates the seasonal control and thus minimizes the operating costs by up to 18 % for pure lime storage and up to 3 % for hybrid configuration. Following the minimum, the deviation with linear power increases abruptly to values beyond $rdev$=5e3, with quadratic power it converges to a limit value. The increase in the slope of the deviation with linear power to very high values is due to the fact that the tracking part is now overweighted and the minimization of the cost function corresponds to the maximization of the lime storage mass. This increase is limited by the maximum power $P_{LS,ch}$ of the lime storage module, which is now continuously applied. This is not the case with a quadratic power of the tracking fraction. In this case, the seasonal control with strict tracking of the base year trajectory minimizes the operating costs by still 5 % for pure lime storage but increases the operating costs by 10 % for hybrid configuration. The deviation minimum $rdev(Conf, m, p)_{min}$ for the ORT approach applied on both configurations are negative $rdev(LS, 1, 10.46e{-}3){=}{-}4.2 \%$, $rdev(LSHP, 2, 1.59e{-}3){=}{-}0.33 \%$. The MPC$_{16}$ and OGS$_{16}$ curve in appendix fig. 14a equal in the initial state but dif-

fer in the final state. This is why the minimum is negative. A correction of the relative deviation by the final state difference is not made, since no comprehensible unambiguous conditions for the final state change could be established. In general, the choice of prefactor has a very sensitive effect on operating costs. These results confirm hypothesis 4, suggesting that there is an optimal weighting between the short-term economic criterion and the long-term tracking criterion.

Finally, the influence of the base year lime storage curve on the relative deviation was investigated. Thereby, the lime storage trajectory was scaled and raised by the factor tuple $\{a, b\}$. The base year lime storage trajectory applied ($m_{LS,by,new}$) was derived from the respective trajectory ($m_{LS,by,old}$) in fig. 8 as follows:

$$m_{LS,by,new}=a\,m_{LS,by,old}+b\,mean(m_{LS,by,old}) \qquad (27)$$

The results in table 5 pertain to simulations with the respective optimal parameter p. The factor tuple $\{a, b\}=\{1, 0\}$ does not change the lime storage curve $m_{LS,by}$. On the other hand, the tuples $\{0.6,0\},\{0,0\},\{0,1\}$ lead to a compressed curve or to a complete lowering to the zero line or to a raised and constant curve, respectively. All these different parameter tuples influence the control behaviour only if the quadratic power was applied. In the case of linear power, the lime storage curve over the year is controlled in the same way, independent of the choice of the factor tuple. Two main statements result from this. First, the linear power approach can do without higher-level lime storage information. It best fits the ideal lime storage trajectory at reference free conditions. All decision information for seasonal storage charging and discharging must thus be available inside the current year prediction horizon of 5 days. Second, for the quadratic power approaches the best control behaviour is revealed with the OGS-generated lime storage trajectory instead of a randomly chosen trajectory. The results show that hypothesis 5 does not hold for this control approach because, at least with a linear power, the current year prediction horizon alone is sufficient to operate the system optimally. A further analysis of the annual lime storage trajectory resulting from different control parameters and heat supply configurations is discussed in the appendix section 7.

4.4. Analysis of the CORT approach

The analysis of the second control approach is carried out varying the final state constraint bound ϵ and the base year prediction horizon t_{by} as depicted in fig. 10 and fig. 11.
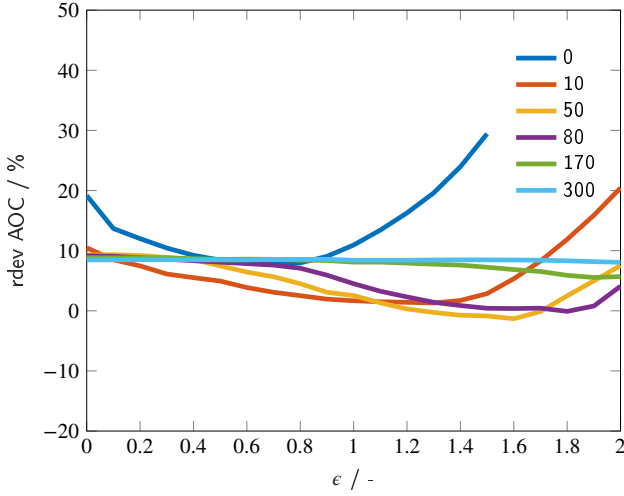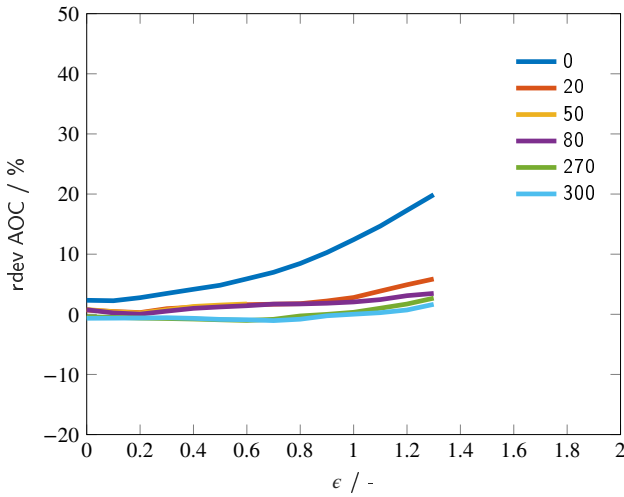
Figure 10: Results of the relative deviation $rdev$ for various bounds ϵ and base year prediction horizons t_{by} applying the CORT approach on the configuration **LS**.

Figure 11: Results of the relative deviation $rdev$ for various bounds ϵ and base year prediction horizons t_{by} applying the CORT approach on the configuration **LSHP**.

Therefore, the parameters where varied with a step width of at least 0.1 for the bound ϵ and 30 days for the prediction horizon t_{by}.

In general, the value $\epsilon=0$, lowers the final state constraint to zero. This corresponds to a reference free MPC approach. An adjustment of the base year prediction horizon $t_{by}=300d$ leads to minimal relative deviations. The original lime storage trajectory is followed with increasing lower bound to $\epsilon=1$. Compared to the reference-free condition, a base-year prediction horizon $t_{by}=10d$ for pure lime-storage supply and $t_{by}=300d$ for hybrid supply now leads to minimal relative deviations. The results at $t_{by}=0d$ correspond to those of the ORT approach at high prefactor. As the lower bound $\epsilon>1$ increases further, a raised lime storage trajectory is followed. For the heat supply configuration LS fig. 10 the relative deviation results reveal a distinct minimum progression up to

prediction horizons of 170 days. The position of the minimum shifts to midrange values around $\epsilon=1.6$. Accordingly, increasing the lime storage quantity at the end of the base-year prediction horizon has a beneficial effect on flexibility and full-year performance. This shows that hypothesis 5 holds at least for the CORT approach and thus a prediction horizon above that of public weather forecasts is needed for efficient operation. The global minimum $rdev(\text{Conf}, \epsilon, t_{by})_{min}$ shows up at $rdev(\text{LS}, 1.6, 50)=-1.3\,\%$. Accordingly, midrange values of the flexibility parameters are optimal. For the heat supply configuration *LSHP* results in fig. 11 depict a very slightly pronounced minimum gradient. The global minimum shows up at $rdev(\text{LSHP}, 0.7, 300)=-1.0\,\%$. Due to the progression, no further points were sampled for values $\epsilon>1.3$. Compared to the *LS* configuration, this difference could be due to the lower amount of lime stored. As depicted in fig. 7 (solid lines), since the hybrid configuration stores lime seasonally at much lower electricity prices than the pure configuration, these times are easier for the controller to hit. Compared to the ORT approach, this deviations are higher and the computational costs several times higher as discussed in section 4. According to this, integrating reference tracking into the objective function instead of the constraints not only leads to lower operating costs but also to significantly lower computation time. This fully confirms hypothesis 3. A further analysis of the annual lime storage trajectory resulting from different control parameters and heat supply configurations is discussed in the appendix section 7.

4.5. Robustness analysis of the ORT approach

Finally, the best possible MPC approach for seasonal lime storage control, the ORT approach with linear power was applied on different weather and electricity price signals by varying the prefactor p to access the robustness of the approach.

Figure 12 and fig. 13 show the relation of the relative deviation depending on the value of the prefactor p, the year of the weather data and the relative fluctuation range of the electricity price signal. As the relative fluctuation range increases, the difference between the relative deviation at a prefactor $p=10e-4$ and at the optimal prefactor increases. This comparison indicates a significant improvement due to the seasonal control with increasing relative fluctuation range $rstd$. It reveals, depending on the relative fluctuation range, savings between 3-50\,% for the *LS* configuration and 0-72\,% for the *LSHP* configuration. In addition to the shift of the minimum to lower values p, the slope of the minimum increases with increasing fluctuation range. This is making the proper choice of the controller parameter more significant. The curves at different weather data differ significantly less than at different relative fluctuation range. The results reveal that the choice of the prefactor very sensitively influences the optimal control of the seasonal energy storage system. Accordingly, the value of the prefactor p must always be readjusted to the current weather and electricity price development within a certain period.
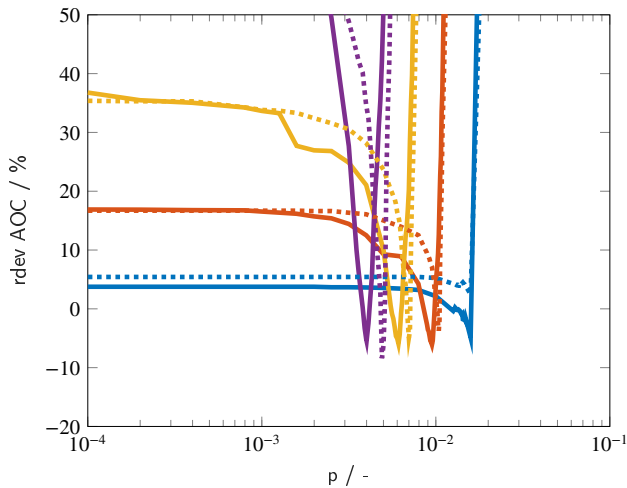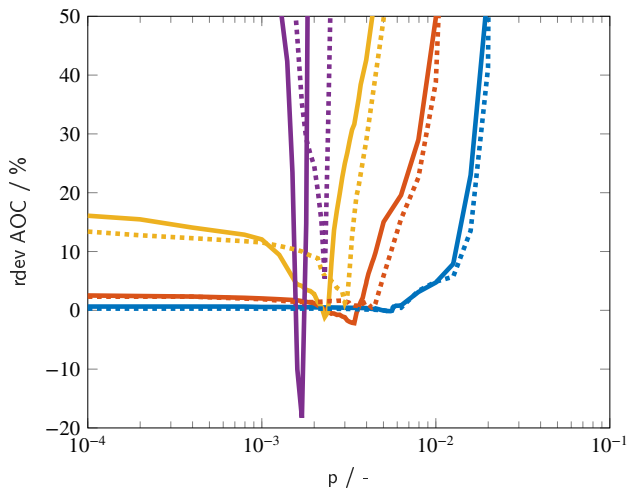
Figure 12: Results of relative deviation versus different values of prefactor *p*, years of weather data (2015 solid, 2016 dotted) and different relative fluctuation ranges **rstd** of electricity price signals (20 %, 30 %, 40 %, 50 %) for the configuration **LS**.

Figure 13: Results of relative deviation versus different values of prefactor *p*, years of weather data (2015 solid, 2016 dotted) and different relative fluctuation ranges **rstd** of electricity price signals (20 %, 30 %, 40 %, 50 %) for the configuration **LSHP**.

5. Conclusion

In this work, models of an energy system consisting of a building, a water buffer and three different heat supply configurations were developed. In addition, two model predictive control concepts were devised to operate the system over a period of one year with the objective of minimizing operating cost. The control approaches include a higher-level annual scheduling and a lower-level dynamic MPC control for flexible trajectory tracking. To approximate weather and electricity price data beyond the public forecast period, TRY weather and mean electricity spot market price data were used in conjunction with a perfectly predicted occupation profile.

The key findings of the study are as follows:

The hybrid integration of a heat pump and a novel lime storage module into the heat supply of a building allows a reduction of operating costs of 18 % in the realistic scenario and up to 80 % in case of highly fluctuating electricity prices. The pure lime storage system *LS* without a heat pump is not economical in any case but could bring other advantages in terms of life cycle costs. Hypothesis 1 can be fully confirmed.

The reduction in AOC associated with seasonal lime storage strongly depends on the relative fluctuation range of the electricity price. Hypothesis 2 needs to be extended to state that weather data and control parameters also influence cost reduction. The robustness of the AOC is distinctly lower with the ORT approach than the CORT approach. It is therefore essential that future control concepts accurately predict the electricity price and weather data to precisely locate optimal control parameter values. For this purpose, a scenario based economic model predictive control approach is proposed which periodically adjusts the controller parameters to the weather and electricity price data.

Compared to the constraint based approach CORT, the objective based approach ORT has a significantly lower computation time (1-2min compared to 1min-30h) and shows at least for the *LS* configuration a better performance compared to the optimal curve with the OGS algorithm OGS_{16}. The AOC resulting from the application of the ORT approach are −4.2 % below the optimal cost, those from the CORT approach are −1.3 %. For the hybrid configuration *LSHP*, the best possible results are closer, −0.33 % ORT and −1 % CORT.

As far as the tracking condition is formulated in the objective function, like in the ORT approach, a unique parameter was established, which describes the weighting between the short-term economic part and the seasonal storage benefit. This weighting parameter is a central component within the approach and influences the AOC very sensitively.

The building with light construction without concrete has a slightly increased energy and cost compared to the concrete construction but has enormous potential savings in life cycle costs and thus supports the objectives of the Collaborative Research Centre SFB1244. Future models should represent the performance of the heat pump in more detail and should include greenhouse gas emissions in the objective function to further investigate the value of the lime storage module, which does not use harmful refrigerants.

Hypothesis 5 applies only to the CORT approach, according to which a prediction horizon greater than that of public forecast periods of about 5 days is needed to successfully operate a seasonal energy storage system. The central conclusion of this work is that the ORT approach can even completely dispense with the application of a two-layer control hierarchy. Future work on the control of seasonal energy storage should take this into account.

6. Acknowledgements

References

[1] United Nations, Paris Agreement, United Nations Treaty Collection, Chapter XXVII 7. d (2016).

[2] Deutsche Bundesregierung, Was tut die Bundesregierung für den Klimaschutz?, 2021. URL: https://www.bundesregierung.de/breg-de/themen/klimaschutz/bundesregierung-klimapolitik-1637146, (German).

[3] AG Energiebilanzen e.V., Private Haushalte sparen bei Raumwärme und Beleuchtung (German), 2020. URL: https://ag-energiebilanzen.de/22-0-Presse-dienst.html.

[4] T. Künzel, Entwicklung eines agentenbasierten Marktmodells zur Bewertung der Dynamik am deutschen Strommarkt in Zeiten eines steigenden Anteils erneuerbarer Energien, 2019. doi:10.5445/IR/1000100456, iSBN: 9781000100457.

[5] J. Lizana, R. Chacartegui, A. Barrios-Padura, J. M. Valverde, Advances in thermal energy storage materials and their applications towards zero energy buildings: A critical review, Applied Energy 203 (2017) 219–239.

[6] P. Tatsidjodoung, N. L. Pierrès, L. Luo, A review of potential materials for thermal energy storage in building applications, Renewable and Sustainable Energy Reviews (2013).

[7] M. Angerer, M. Becker, S. Härzschel, K. Kröper, S. Gleis, A. Vandersickel, H. Spliethoff, Design of a MW-scale thermo-chemical energy storage reactor, Energy Reports (2018).

[8] J. Drgoňa, J. Arroyo, I. Cupeiro Figueroa, D. Blum, K. Arendt, D. Kim, E. P. Ollé, J. Oravec, M. Wetter, D. L. Vrabie, L. Helsen, All you need to know about model predictive control for buildings, Annual Reviews in Control 50 (2020) 190–232.

[9] C. Finck, R. Li, R. Kramer, W. Zeiler, Quantifying demand flexibility of power-to-heat and thermal energy storage in the control of building heating systems, Applied Energy (2018).

[10] C. R. Touretzky, M. Baldea, A hierarchical scheduling and control strategy for thermal energy storage systems, Energy and Buildings (2016).

[11] Q. Xu, S. Dubljevic, Model predictive control of solar thermal system with borehole seasonal storage, Computers and Chemical Engineering (2017).

[12] M. Jonin, M. Khosravi, A. Eichler, W. Villasmil, P. Schuetz, C. N. Jones, R. S. Smith, Exergy-based model predictive control for design and control of a seasonal thermal energy storage system, Journal of Physics: Conference Series (2019).

[13] M. Fiorentini, J. Wall, Z. Ma, J. H. Braslavsky, P. Cooper, Hybrid model predictive control of a residential HVAC system with on-site thermal energy generation and storage, Applied Energy (2017).

[14] J. Široký, F. Oldewurtel, J. Cigler, S. Prívara, Experimental analysis of model predictive control for an energy efficient building heating system, Applied Energy (2011).

[15] C. Finck, R. Li, W. Zeiler, An optimization strategy for scheduling various thermal energy storage technologies in office buildings connected to smart grid, Energy Procedia (2015). 6th International Building Physics Conference, IBPC 2015.

[16] M. Petrollese, L. Valverde, D. Cocco, G. Cau, J. Guerra, Real-time integration of optimal generation scheduling with MPC for the energy management of a renewable hydrogen-based microgrid, Applied Energy (2016).

[17] A. Lefort, R. Bourdais, G. Ansanay-Alex, H. Guéguen, Hierarchical control method applied to energy management of a residential house, Energy and Buildings (2013).

[18] D. Sturzenegger, D. Gyalistras, V. Semeraro, M. Morari, R. S. Smith, BRCM Matlab Toolbox: Model generation for model predictive building control, American Control Conference (2014).

[19] D. Sturzenegger, Model predictive building climate control - Steps towards practice, Ph.D. thesis, Automatic Control Laboratory, ETH Zurich, 2014. doi:10.3929/ethz-a-010379191.

[20] DIN Deutsches Institut für Normung e.V., DIN EN ISO 6946-3, Wärmedurchlasswiderstand und Wärmedurchgangskoeffizient - Berechnungsverfahren, Technical Report, Beuth Verlag GmbH, 2018. doi:10.31030/2518301.

[21] A. Kleiner, G. Kasparek, D6.4 Thermophysikalische Stoffwerte von Kälte- und Wärmedämmstoffen, in: VDI-Heatatlas, Springer, 2019, pp. 679–685. URL: https://doi.org/10.1007/978-3-662-52989-8_32.

[22] M. H. Spitzner, D6.5 Wärmeleitfähigkeit von Erdreich, Holz, Holzwerkstoffen, allgemeinen Baustoffen und Mauerwerk, in: VDI-Heatatlas, Springer, 2019, pp. 687–706. URL: https://doi.org/10.1007/978-3-662-52989-8_34.

[23] DIN Deutsches Institut für Normung e.V., DIN EN ISO 52016-1, Energetische Bewertung von Gebäuden- Energiebedarf für Heizung und Kühlung, Innentemperaturen sowie fühlbare und latente Heizlasten-Teil1: Berechnungsverfahren, Technical Report, Beuth Verlag GmbH, 2018. doi:10.31030/2577376.

[24] DIN Deutsches Institut für Normung e.V., DIN V 18599-10, Energetische Bewertung von Gebäuden – Berechnung des Nutz-, End- und Primärenergiebedarfs für Heizung, Kühlung, Lüftung, Trinkwarmwasser und Beleuchtung – Teil 10: Nutzungsrandbedingungen, Klimadaten, Technical Report, Beuth Verlag GmbH, 2018. doi:10.31030/2874436.

[25] VDI-Gesellschaft Bauen und Gebäudetechnik (GBG), VDI 6007 Blatt 1 - Berechnung des instationären thermischen Verhaltens von Räumen und Gebäuden - Raummodell, Technical Report, Verein Deutscher Ingenieure e.V, 2015.

[26] Bosch Thermotechnology GmbH, Bosch climate 5000 Singlesplit-Device, 2021. URL: https://www.bosch-thermotechnology.com/de/de/ocs/wohngebaeude/climate-5000-1150265-p/.

[27] DIN Deutsches Institut für Normung e.V., DIN V 18599-8, Energetische Bewertung von Gebäuden – Berechnung des Nutz-, End- und Primärenergiebedarfs für Heizung, Kühlung, Lüftung, Trinkwarmwasser und Beleuchtung – Teil 8: Nutz- und Endenergiebedarf von Warmwasserbereitungssystemen, Technical Report, Beuth Verlag GmbH, 2018. doi:10.31030/2878217.

[28] M. Schmidt, M. Linder, A Novel Thermochemical Long Term Storage Concept: Balance of Renewable Electricity and Heat Demand in Buildings, Frontiers in Energy Research (2020).

[29] 12th REHVA World Congress (CLIMA 2016) (Ed.), Operational load shaping of office buildings connected to thermal energy storage using dynamic programming, 2016.

[30] T. Huld, R. Müller, A. Gambardella, A new solar radiation database for estimating PV performance in Europe and Africa, Solar Energy (2012).

[31] Bundesnetzagentur, German electricity market data, 2021. URL: https://www.smard.de.

[32] J. A. E. Andersson, J. Gillis, G. Horn, J. B. Rawlings, M. Diehl, CasADi – A software framework for nonlinear optimization and optimal control, Mathematical Programming Computation (2019).

[33] S. Weber, Model predictive approaches for building climate and seasonal energy storage control, 2020. doi:10.18419/opus-10923, Master's thesis.

[34] STATISTICAL OFFICE OF THE EUROPEAN COMMUNITIES EUROSTAT, Electricity prices for non-household consumers, 2021. URL: https://ec.europa.eu/eurostat/databrowser/view/nrg_pc_205/default/table?lang=en.

7. Appendix

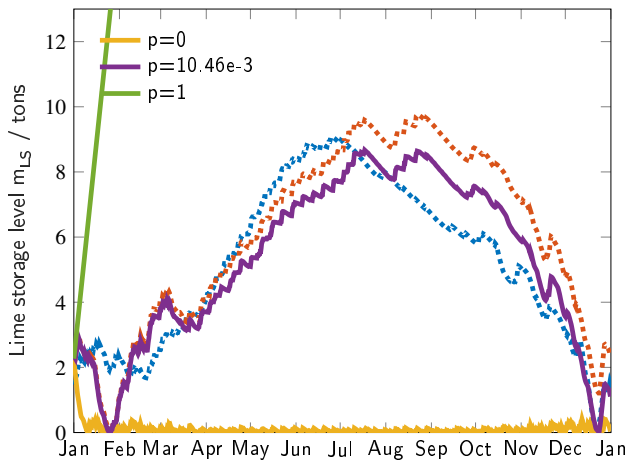Figure 14 depicts the annual lime storage trajectories MPC_{16} of different control approaches, system configurations and control parameters. Optimal trajectories OGS_{by} and OGS_{16}
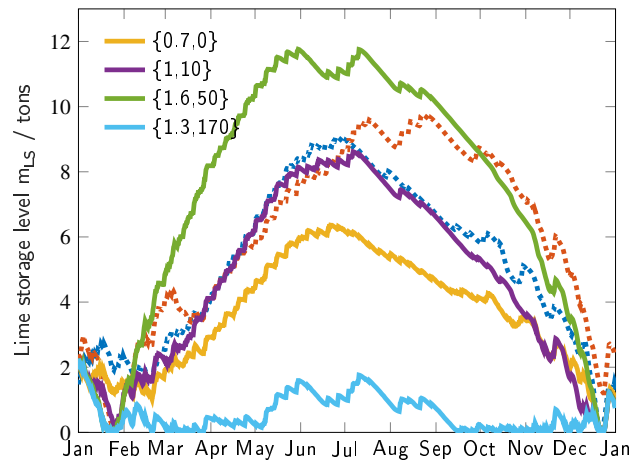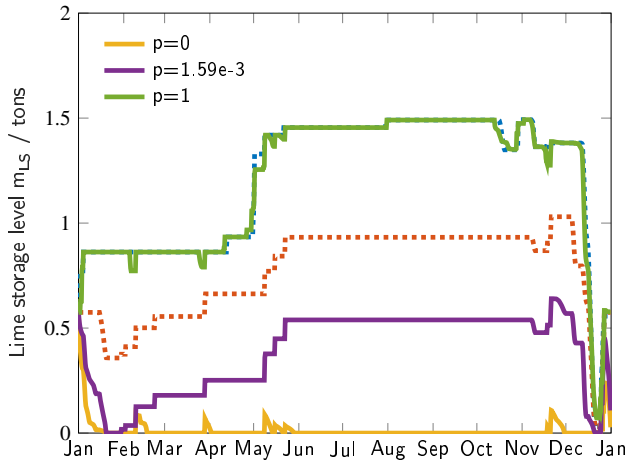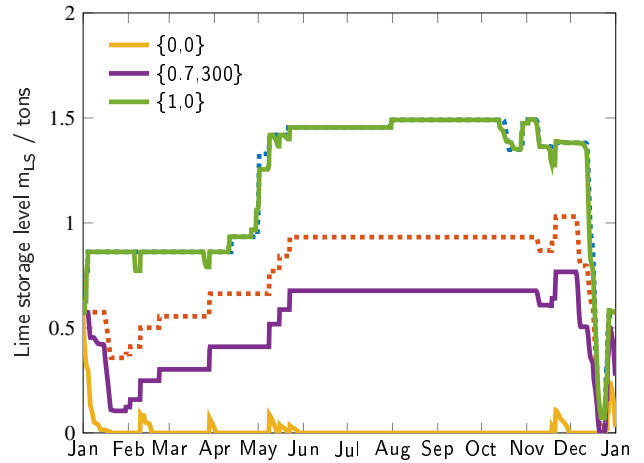
(a) Approach **ORT**, configuration *LS*, parameter $m=1$

(b) Approach **CORT**, configuration *LS*, parameter set $\{\epsilon, t_{by}\}$

(c) Approach **ORT**, configuration *LS*, parameter $m=2$

(d) Approach **CORT**, configuration *LS*, parameter set $\{\epsilon, t_{by}\}$

Figure 14: Annual lime storage trajectories MPC_{16} of different control approaches, system configurations and control parameters. Optimal trajectories OGS_{by} (dotted) and OGS_{16} (dotted)

are generated by the OGS algorithm with 2016 and base year disturbance data, respectively.

Figure 14a depicts the results for ORT approach and pure lime storage configuration *LS* at linear power parameter. For a prefactor of $p=0$, due to the undervaluation of the lime storage mass within the objective function no lime is stored during the year. The maximization of the lime storage mass at $p=1$ is shown by the rapid increase of the lime storage mass. The curve with an optimally selected parameter $p=10.46e{-}3$ clearly breaks away from the base year curve follows the OGS_{16} curve. In contrast, the best possible trajectory in fig. 14b based on the CORT approach rises significantly above the OGS_{16} curve at the beginning of the year and drops below it in October. The increase is due to the choice of the parameter ϵ, which raises the curve. This difference leads to higher annual operating costs.

Figure 14c depicts the results for ORT approach and hybrid configuration *LSHP* at quadratic power parameter. The trajectory at $p=0$ corresponds to that of the pure configuration *LS*. The curve at $p=1$ in conjunction with the quadratic power parameter ensures a strict trajectory sequence. The

two equally coloured curves in fig. 14d show the same progression. The two optimal trajectories are similar to each other because the annual operating costs are approximately the same.